

Supporting Information

Yang et al. 10.1073/pnas.1301331110

SI Methods

Mice. Female 8- to 12-wk-old C57BL/6 mice were bred, acclimated, and caged in a group of six or fewer mice per cage at the animal facility of the Department of Microbiology, Tumor and Cell Biology, Karolinska Institute. Mice were killed by a lethal dose of CO₂, followed by cervical dislocation. All animal studies were approved by the Karolinska Institutet local ethical committee and the Northern Stockholm Experimental Animal Ethical Committee.

Treatment with VEGF and VEGFR Blockades. A rabbit anti-mouse VEGF-specific neutralizing antibody (BD0801) was kindly provided by the Simcere Pharmaceutical Company (Nanjing, Jiangsu, China) (1). Rat specific antibodies to mouse VEGF receptor (VEGFR)-1 (MF1) and to mouse VEGFR-2 (DC101) (2–4) were kindly provided by ImClone Systems. These antibodies were intraperitoneally (i.p.) injected twice per week into each of the mice at the dose of 5 mg/kg of the anti-VEGF antibody and 200 µg per mouse of anti-VEGFR-1 or anti-VEGFR-2 antibodies ($n = 6$ mice per group). Tissue samples were collected at the end of the experimental duration. In the discontinuation experiment, VEGF blockade was injected i.p. two times/week into each of the mice at the dose of 5 mg/kg ($n = 6$ mice per group). Tissue samples were collected at various time points after cessation of anti-VEGF treatment, including day 0, 7, 14, and 28. For dose-dependent experiments, VEGF blockade was injected i.p. two times per week into each of the mice at the doses of 1.25, 5, and 15 mg/kg ($n = 6$ mice per group).

Tissue, Blood and Organ Collection. Mice were killed after 2 wk of antibody administration. Necropsy was performed, and various tissues and organs were removed and immediately fixed with 4% (wt/vol) Paraformaldehyde (PFA) overnight, followed by washing with PBS. A fraction of the tissues and organs was embedded with paraffin until further use. Blood samples were collected from anti-VEGF and control animals using an intracardial method (2, 3), and serum samples were kept at -20°C until further use.

Histological Studies and Whole-Mount Staining. Paraffin-embedded tissues were sectioned at a thickness of 5 µm and stained with H&E as described (5). Whole-mount staining was performed according to our published methods (6–11). Briefly, small pieces of tissues were cut into thin slices and fixed in 4% (wt/vol) PFA overnight, followed by treatment with proteinase K (20 µg/mL). Tissues were incubated with primary antibodies overnight at 4 °C, followed by staining with secondary antibodies for 2 h at room temperature. Necessary washes with PBS were performed in between or after staining. Slides were mounted and examined under a confocal microscope (Zeiss Confocal LSM510 Microscope). By scanning 10 thin sections at 4- to 5-µm distances of each sample, three-dimensional images of each tissue sample were projected. Quantitative analyses from at least eight different tissue sections were performed using Adobe Photoshop CS software program.

Immunofluorescence Staining. Paraffin-embedded slides were prepared at 5 µm and baked at 60 °C overnight. Antigen retrieval was achieved with an unmasking solution (Vector Labs; H3300). Bone samples were preheated for 2.5 min in a microwave oven at the maximal power and then heated for 5.5 min at 20% power. For soft samples, prolonged heating was used. Samples were

chilled to room temperature, followed by washing twice with PBS for 5 min. Samples were treated with blocking buffer [4% (vol/vol) goat serum in PBS] at room temperature for 30 min. A rat anti-mouse endomucin (eBioscience; cat. no. 14–5851-85, clone eBioV.7C7) antibody (1:200 dilution in blocking buffer) was used for incubation at 4 °C overnight. A secondary antibody (goat anti-rat Alexa 555; Invitrogen; cat. no. A21434; 1:400 dilution) in the blocking buffer was incubated at room temperature for 45 min. For apoptosis assay, a rabbit anti-mouse cleaved caspase-3 antibody (Cell Signaling; cat. no. 9661; 1:200 dilution in a blocking buffer) and a secondary antibody (donkey anti-rabbit Alexa 488; Invitrogen; cat. no. A21206; 1:400 dilution) were used. Slides were mounted with Vectashield (Vector Laboratories; cat. no. H-1000) and kept in -20°C .

Vascular Perfusion Assay. Anti-VEGF-treated and nontreated mice were anesthetized and were injected into the tail vein with a lysinated fluorescein-labeled dextran (2,000 kDa; 100 µL per mouse; Invitrogen) (12). After 10 min, animals were killed, and tissues and organs were dissected and immediately fixed with 4% (wt/vol) PFA at 4 °C. Thyroids were carefully dissected, whole-mount stained, and examined by confocal microscopy.

Western Blot. After 2-wk anti-VEGF treatment, mice were anesthetized and i.v. injected with 1.5 mg pimonidazole (Hypoxyprobe). Mice were killed 15 min later, and thyroid was resected and immediately lysed. Total protein samples were collected. Fifteen micrograms of total protein was loaded into each channel and separated using a 10% (wt/vol) SDS/PAGE gel and then transferred onto a nitrocellulose membrane. Membranes were probed overnight at 4 °C with a mouse anti-pimonidazole monoclonal antibody (clone 4.3.11.3, Hypoxyprobe) and diluted in PBS with 5% (wt/vol) BSA containing 0.1% Tween 20, as recommended by the manufacturer. The membrane was incubated for 1 h with a donkey anti-mouse IgG antibody (IRDye 680RD; LI-COR; 1:15000). Protein bands were visualized and quantified using ODYSSEY CLx (LI-COR) at 700 nm wavelength.

ELISA. Serum levels of mouse free triiodothyronine (T3) and free thyroxine (T4) were measured and quantified by using an ELISA method according to the manufacturer's instructions (cat. nos. MBS705057 and MBS162146; Mybiosource).

Electron Microscopy. After 2-wk anti-VEGF antibody treatment, animals were killed and immediately fixed with 2.5% (vol/vol) glutaraldehyde plus 1% paraformaldehyde in 0.1 M phosphate buffer (pH 7.4) by vascular perfusion. Thyroids were dissected and fixed with a fresh fixative. Electron microscopy examination and image captures were obtained as previously described (13, 14). Ultrathin tissue sections in 40–50 nm were prepared and examined in a Tecnai 12 Spirit Bio TWIN transmission electron microscope (Fei Company) at 100 kV. Digital images were taken by using a Veleta camera (Olympus Soft Imaging Solutions).

Statistical Analysis. For quantitative analysis, randomized micrographs from at least eight different fields were used. Six animals were recruited to each group, and each experiment was repeated three times. The Adobe Photoshop CS4 software program was used with a color range tool and a count tool to detect positive areas or numbers. Statistical analyses were performed using the standard two-tailed Student *t* test, and values of $P < 0.05$, $P < 0.01$, and $P < 0.001$ were deemed statistically significant.

1. Yu YL, et al. (2010) A humanized anti-VEGF rabbit monoclonal antibody inhibits angiogenesis and blocks tumor growth in xenograft models. *PLoS ONE* 5(2):e9072.
2. Xue Y, et al. (2008) Anti-VEGF agents confer survival advantages to tumor-bearing mice by improving cancer-associated systemic syndrome. *Proc Natl Acad Sci USA* 105(47):18513–18518.
3. Zhang D, et al. (2011) Antiangiogenic agents significantly improve survival in tumor-bearing mice by increasing tolerance to chemotherapy-induced toxicity. *Proc Natl Acad Sci USA* 108(10):4117–4122.
4. Cao R, et al. (2010) VEGFR1-mediated pericyte ablation links VEGF and PIGF to cancer-associated retinopathy. *Proc Natl Acad Sci USA* 107(2):856–861.
5. Xue Y, et al. (2012) PDGF-BB modulates hematopoiesis and tumor angiogenesis by inducing erythropoietin production in stromal cells. *Nat Med* 18(1):100–110.
6. Cao R, et al. (2012) Collaborative interplay between FGF-2 and VEGF-C promotes lymphangiogenesis and metastasis. *Proc Natl Acad Sci USA* 109(39):15894–15899.
7. Zhang F, et al. (2012) Proliferative and survival effects of PUMA promote angiogenesis. *Cell Rep* 2(5):1272–1285.
8. Jensen LD, et al. (2012) Opposing effects of circadian clock genes *bmal1* and *period2* in regulation of VEGF-dependent angiogenesis in developing zebrafish. *Cell Rep* 2(2): 231–241.
9. Lim S, et al. (2012) Cold-induced activation of brown adipose tissue and adipose angiogenesis in mice. *Nat Protoc* 7(3):606–615.
10. Cao R, et al. (2011) Mouse corneal lymphangiogenesis model. *Nat Protoc* 6(6): 817–826.
11. Xue Y, Lim S, Bråkenhielm E, Cao Y (2010) Adipose angiogenesis: Quantitative methods to study microvessel growth, regression and remodeling in vivo. *Nat Protoc* 5(5):912–920.
12. Hedlund EM, et al. (2013) Tumor cell-derived placental growth factor sensitizes antiangiogenic and antitumor effects of anti-VEGF drugs. *Proc Natl Acad Sci USA* 110(2):654–659.
13. Al-Hashmi S, et al. (2012) Busulphan-cyclophosphamide cause endothelial injury, remodeling of resistance arteries and enhanced expression of endothelial nitric oxide synthase. *PLoS ONE* 7(1):e30897.
14. Eriksson A, et al. (2003) Small GTP-binding protein Rac is an essential mediator of vascular endothelial growth factor-induced endothelial fenestrations and vascular permeability. *Circulation* 107(11):1532–1538.

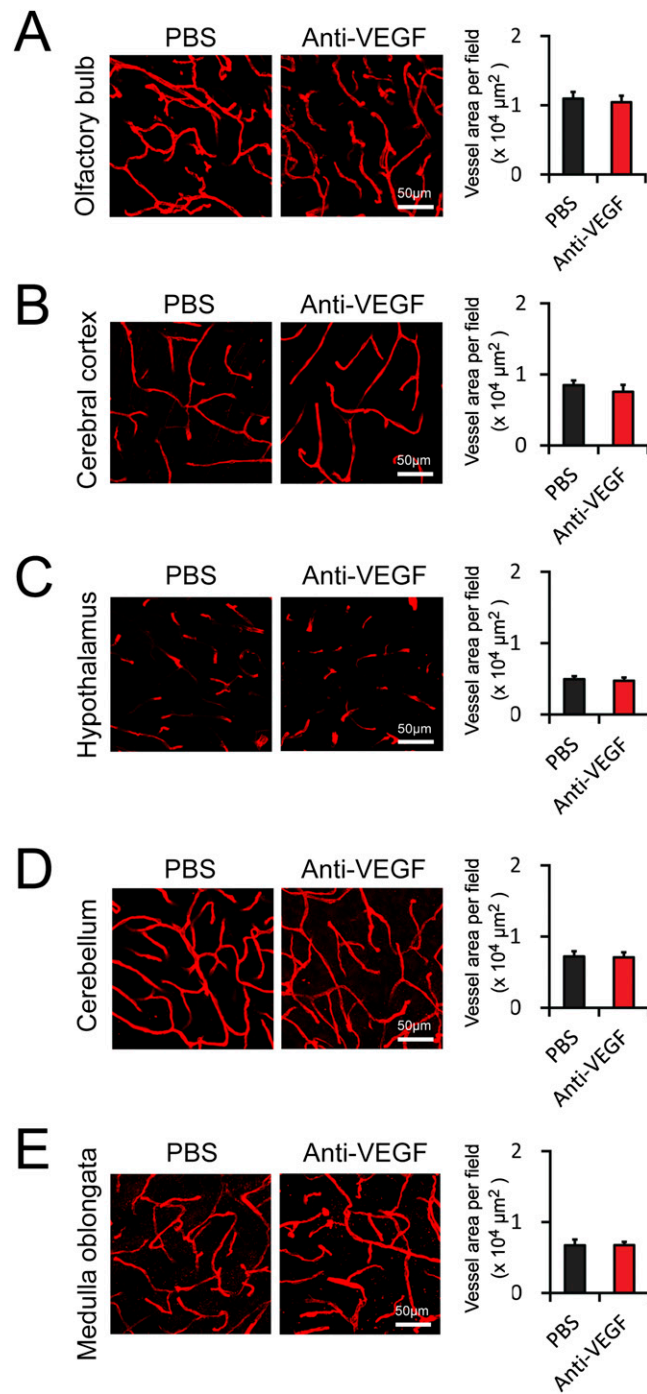


Fig. S1. Impact of anti-VEGF antibody treatment on vasculature in brain. (A) CD31⁺ olfactory bulb microvessels (red). Vessel areas were quantified (20× magnification, $n = 8$ per group). (B) CD31⁺ cerebral cortex microvessels (red). Vessel areas were quantified (20× magnification, $n = 8$ per group). (C) CD31⁺ hypothalamus microvessels (red). Vessel areas were quantified (20× magnification, $n = 8$ per group). (D) CD31⁺ cerebellum microvessels (red). Vessel areas were quantified (20× magnification, $n = 8$ per group). (E) CD31⁺ medulla oblongata microvessels (red). Vessel areas were quantified (20× magnification, $n = 8$ per group). Data are presented as means \pm SEM.

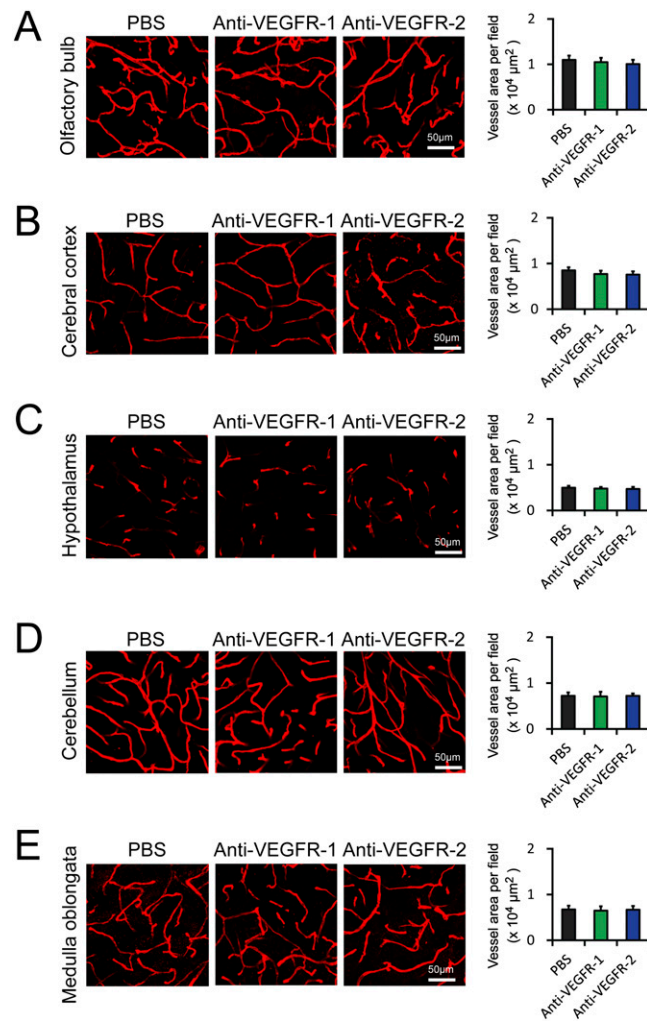


Fig. 52. Impact of anti-VEGFR-1 and anti-VEGFR-2 antibody treatment on vasculature in brain. (A) CD31⁺ olfactory bulb microvessels (red). Vessel areas were quantified (20× magnification, $n = 8$ per group). (B) CD31⁺ cerebral cortex microvessels (red). Vessel areas were quantified (20× magnification, $n = 8$ per group). (C) CD31⁺ hypothalamus microvessels (red). Vessel areas were quantified (20× magnification, $n = 8$ per group). (D) CD31⁺ cerebellum microvessels (red). Vessel areas were quantified (20× magnification, $n = 8$ per group). (E) CD31⁺ medulla oblongata microvessels (red). Vessel areas were quantified (20× magnification, $n = 8$ per group). Data are presented as means \pm SEM.

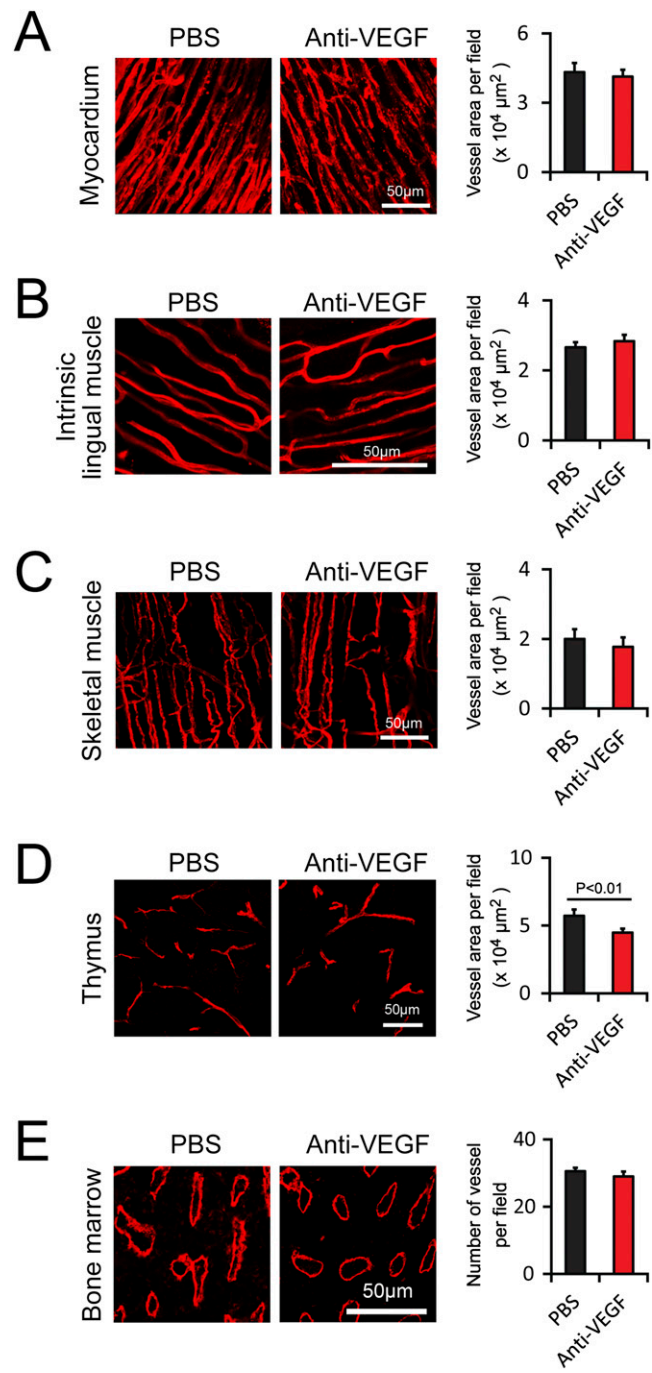


Fig. S3. Impact of anti-VEGF antibody treatment on vasculature in muscle, thymus, and bone marrow. (A) CD31⁺ myocardium microvessels (red). Vessel areas were quantified (20 \times magnification, $n = 8$ per group). (B) CD31⁺ intrinsic lingual muscle microvessels (red). Vessel areas were quantified (20 \times magnification, $n = 8$ per group). (C) CD31⁺ skeletal muscle microvessels (red). Vessel areas were quantified (20 \times magnification, $n = 8$ per group). (D) CD31⁺ thymus microvessels (red). Vessel areas were quantified (20 \times magnification, $n = 8$ per group). (E) Endomucin⁺ bone marrow microvessels were detected in paraffin-embedded (red). Vessel areas were quantified (20 \times magnification, $n = 8$ per group). Data are presented as means \pm SEM.

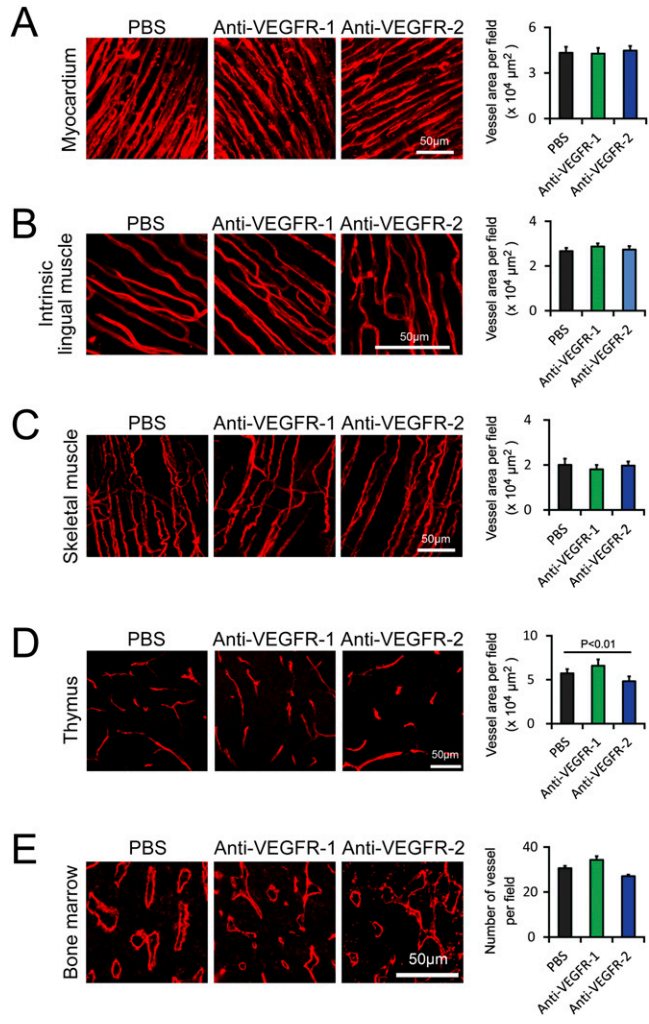


Fig. 54. Impact of anti-VEGFR-1 and anti-VEGFR-2 antibody treatment on vasculature in muscle, thymus, and bone marrow. (A) CD31⁺ myocardium microvessels (red). Vessel areas were quantified (20 \times magnification, *n* = 8 per group). (B) CD31⁺ intrinsic lingual muscle microvessels (red). Vessel areas were quantified (20 \times magnification, *n* = 8 per group). (C) CD31⁺ skeletal muscle microvessels (red). Vessel areas were quantified (20 \times magnification, *n* = 8 per group). (D) CD31⁺ thymus microvessels (red). Vessel areas were quantified (20 \times magnification, *n* = 8 per group). (E) Endomucin⁺ bone marrow microvessels were detected in paraffin-embedded (red). Vessel areas were quantified (20 \times magnification, *n* = 8 per group). Data are presented as means \pm SEM.

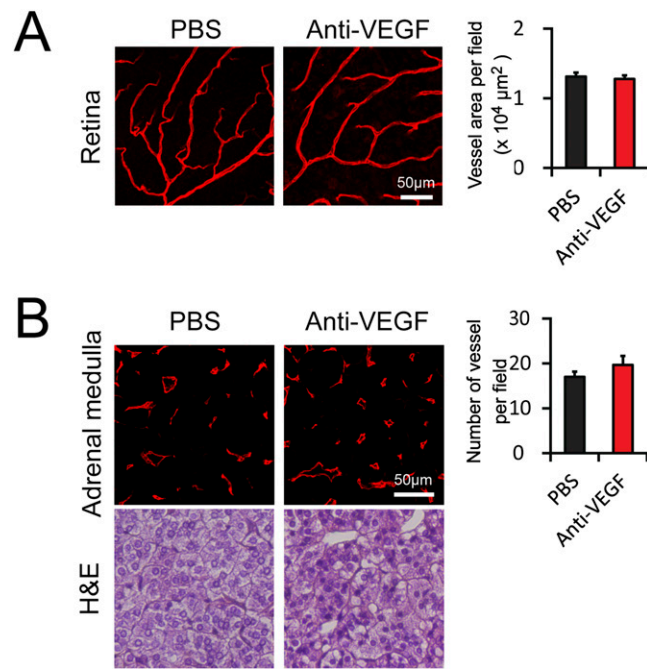


Fig. 55. Impact of anti-VEGF antibody treatment on vasculature in retina and adrenal medulla. (A) CD31⁺ retina microvessels (red). Vessel areas were quantified (20 \times magnification, $n = 8$ per group). (B) Endomucin⁺ adrenal medulla microvessels were detected in paraffin-embedded tissues (red). H&E staining was used to reveal tissue structures. Vessel numbers were quantified (20 \times magnification, $n = 8$ per group). Data are presented as means \pm SEM.

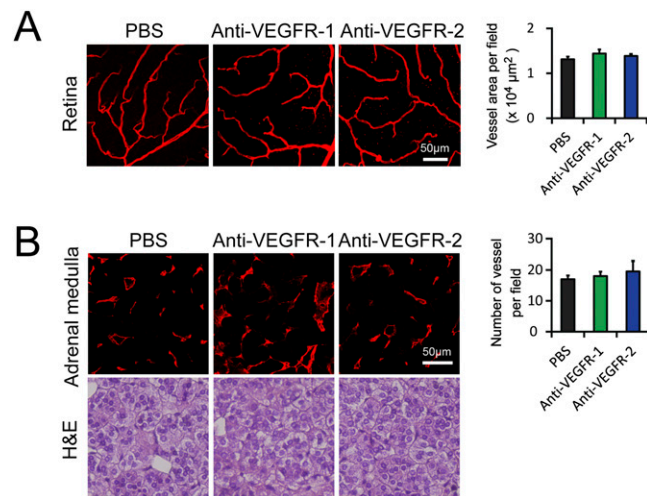


Fig. 56. Impact of anti-VEGFR-1 and anti-VEGFR-2 antibody treatment on vasculature in retina and adrenal medulla. (A) CD31⁺ retina microvessels (red). Vessel areas were quantified (20 \times magnification, $n = 8$ per group). (B) Endomucin⁺ adrenal medulla microvessels were detected in paraffin-embedded tissues (red). H&E staining was used to reveal tissue structures. Vessel numbers were quantified (20 \times magnification, $n = 8$ per group). Data are presented as means \pm SEM.